New Journal of Physics
The open access journal at the forefront of physics

Deutsche Physikalische Gesellschaft DPG IOP Institute of Physics

PAPER • OPEN ACCESS

# Unfolding tagged particle histories in single-file diffusion: exact single- and two-tag local times beyond large deviation theory

To cite this article: Alessio Lapolla and Aljaž Godec 2018 *New J. Phys.* **20** 113021



New Journal of Physics
The open access journal at the forefront of physics

Deutsche Physikalische Gesellschaft DPG
IOP Institute of Physics

Published in partnership with: Deutsche Physikalische Gesellschaft and the Institute of Physics

OPEN ACCESS

RECEIVED
13 July 2018

REVISED
4 October 2018

ACCEPTED FOR PUBLICATION
22 October 2018

PUBLISHED
14 November 2018



PAPER

# Unfolding tagged particle histories in single-file diffusion: exact single- and two-tag local times beyond large deviation theory

**Alessio Lapolla and Aljaž Godec**

Mathematical Biophysics Group, Max-Planck-Institute for Biophysical Chemistry, Göttingen D-37077, Germany

**E-mail:** agodec@mpibpc.mpg.de

**Keywords:** stochastic processes, occupation time functional, single-file diffusion, projection-induced memory, stochastic many-body systems, generating functional, large deviations

## Abstract

Strong positional correlations between particles render the diffusion of a tracer particle in a single file anomalous and non-Markovian. While ensemble average observables of tracer particles are nowadays well understood, little is known about the statistics of the corresponding functionals, i.e. the time-average observables. It even remains unclear how the non-Markovian nature emerges from correlations between particle trajectories at different times. Here, we first present rigorous results for fluctuations and two-tag correlations of general bounded functionals of ergodic Markov processes with a diagonalizable propagator. They relate the statistics of functionals on arbitrary time-scales to the relaxation eigenspectrum. Then we study tagged particle local times—the time a tracer particle spends at some predefined location along a single trajectory up to a time $t$. Exact results are derived for one- and two-tag local times, which reveal how the individual particles' histories become correlated at higher densities because each consecutive displacement along a trajectory requires collective rearrangements. Our results unveil the intricate meaning of projection-induced memory on a trajectory level, invisible to ensemble-average observables, and allow for a detailed analysis of single-file experiments probing tagged particle exploration statistics.

## 1. Introduction

Single-file dynamics refers to the motion of particles in a narrow, effectively one-dimensional channel, which prevents their crossing, and is central to the transport in biological channels [1] the kinetics of transcription regulation [2], transport in zeolites [3] and in superionic conductors [4]. Recent advances in single-particle tracking and nanofluidics enabled experimental studies of single file dynamics in colloidal systems, which directly probe the fundamental physical principles of tagged particle motion to an unprecedented precision [5, 6].

The motion of particles in a single file is strongly correlated, which gives rise to a rich and intricate phenomenology. In a Brownian single file the non-crossing constraint leads to subdiffusion with the ensemble mean squared displacement (MSD) of a tagged particle scaling as $\langle [x(t) - x(0)]^2 \rangle \propto \sqrt{t}$ [7]. When confined to a finite interval the subdiffusive scaling of the MSD is transient, saturating at an equilibrium variance, with the extent of the subdiffusive regime growing with the particle density (see figure 1(a) and [8]). Concurrently, an effective harmonization emerges at increasing density, with the invariant measure of a tagged particle approaching a Gaussian and a vanishing kurtosis excess $\gamma_2 = \langle x^4 \rangle_{\rm eq} / \langle x^2 \rangle_{\rm eq}^2 - 3$ (see inset of figure 1(a)). More generally it holds that the MSD of a tagged particle in an unconfined single file and the absolute dispersion of a free particle in the limit $t \to \infty$ are related via $\langle [x(t) - x(0)]^2 \rangle \propto \langle |x(t)| \rangle_{\rm free}$ [9]. The motion of particles on a many-body level is Markovian, the resulting tagged particle dynamics is, however, highly non-Markovian [8], and displays a staggering dependence on the respective initial conditions [10].

Tremendous effort has been made to study the tagged particle dynamics theoretically [11]. In particular, the tagged particle ensemble propagator has been studied using the 'reflection principle' [12], Jepsen mapping [13], momentum Bethe ansatz [8], harmonization techniques [14], and macroscopic fluctuation [15] and large

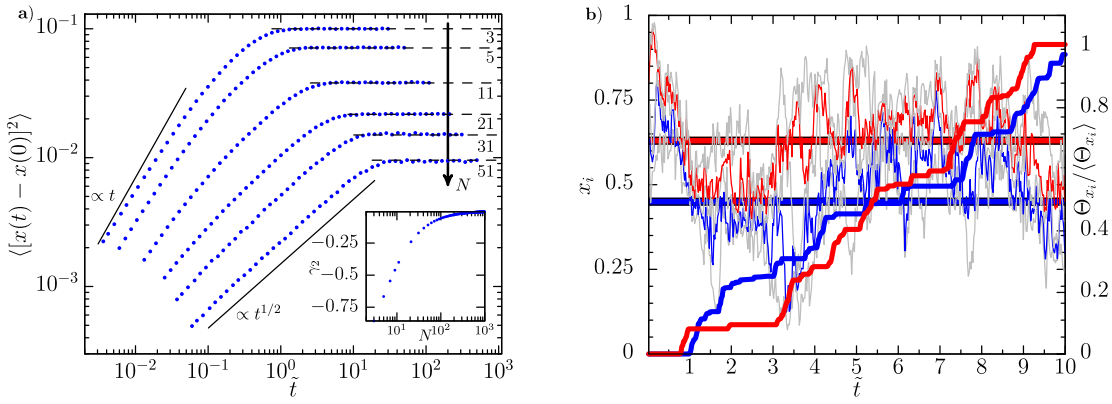


**Figure 1.** (a) MSD of the central particle in a single file with increasing particle number $N$ starting from equilibrium initial conditions. Time is measured in units of the mean number of collisions $\tilde{t} = Dt/N^2$. Inset: Kurtosis excess of the invariant measure of the central particle depending on $N$; (b) trajectories of two next-nearest neighbor particles in a single file of 11 particles (red and blue curves) alongside the respective left and right nearest neighbors (gray curves). Overlaid are corresponding local time fractions up to a time $t$, $\theta_t^i$ in the respective red and blue shaded intervals. The remaining particle trajectories are omitted for convenience.

deviation (LD) [16] theory. Notwithstanding, these works, with isolated exceptions [17], focused on ensemble-average properties alone. State-of-the-art experiments, however, albeit probing particle trajectories and thereby providing direct access to functionals of paths, are typically analyzed using ensemble-average concepts (see e.g. [5, 6]). The analysis of functionals of tagged particle trajectories is thus not only feasible but also more natural than studying ensemble-average observables. Moreover, to arrive at a deeper physical understanding of projection-induced memory effects and resulting non-Markovianity, an understanding of the correlations of particle histories and their decorrelation on ergodic time-scales is required.

In particular, we here focus on the trajectory-, or time-average analogue of the tagged particle ensemble propagator [8]. Any time-average observable can be constructed from the local time fraction (see equation (A4) in appendix A), which is defined as (see figure 1(b))

$$\theta_t^j(y) = t^{-1}\int_0^t \mathbb{1}_y^j[\mathbf{x}(\tau)]\,\mathrm{d}\tau, \tag{1}$$

where $\mathbb{1}_y^j[\mathbf{x}(\tau)] = 1$ if $x_j \in \mathrm{d}y$ centered at $y$, and zero otherwise [18]. $\theta_t^j(y)$ in equation (1) is a random quantity denoting the fraction of the local time, $t\theta_t^j(y)$ — the time the tagged particle $j$ spends in an infinitesimal region around the point $y$ along a trajectory up until time $t$. $\mathbf{x}(t) \equiv (x_1(t), \ldots, x_N(t))^T$ denotes the many-body trajectory written in vector form. The dynamics of a tagged particle $x_i(t)$ irrespective of the other $N-1$ is not Markovian, and any two tagged particle trajectories $x_i(t)$ and $x_j(t)$ are correlated on all but ergodically long times. We focus on the fluctuations and two-tag correlations of local time fractions

$$\sigma^2_{x_i}(t) = \langle\theta_t^i(x)^2\rangle - \langle\theta_t^i(x)\rangle^2, \tag{2}$$

$$\mathcal{C}^{ij}_{xy}(t) = \langle\theta_t^i(x)\theta_t^j(y)\rangle - \langle\theta_t^i(x)\rangle\langle\theta_t^j(y)\rangle, \tag{3}$$

where $\langle\cdots\rangle$ denotes the average over all $N$-particle trajectories starting from the steady-state (in this case Boltzmann equilibrium) and propagating up to time $t$. Note that for ergodic Markov dynamics $\lim_{t\to\infty}\sigma^2_{x_i}(t) = 0$ and $\lim_{t\to\infty}\mathcal{C}^{ij}_{xy}(t) = 0$, reflecting the fact that on ergodically long time-scales time-average observables become deterministic and correlations between them vanish.

A general theory of local times in such correlated non-Markovian dynamics so far remained elusive. And while the statistics of functionals of the form in equation (1) in one-dimensional stochastic processes have been studied extensively in a variety of fields [19, 20], studies of tagged particle functionals in interacting many-body systems are sparse, and mostly limited to extreme value statistics of vicious walkers (see e.g. [21]).

Here, we present rigorous results for variances and two-tag correlations of bounded functionals[1] of Markovian dynamics on arbitrary time-scales, in terms of the relaxation eigenspectrum of the corresponding propagator. The theory also covers the case, when a higher-dimensional dynamics is projected onto a smaller subspace thereby leading to non-Markovian dynamics on the reduced subspace, a hallmark example thereof being tagged-particle dynamics in a single file. The theory applies to all ergodic Markovian systems with a diagonalizable propagator. As an example we study tagged particle local times in a single file of Brownian point particles in a box. Diagonalizing the many-body propagator using the coordinate Bethe ansatz, our results uncover non-Poissonian trajectory-to-trajectory fluctuations of local times, and a cross-over from negatively to

[1] We consider functionals $V[\mathbf{x}(t)]$ of Markovian trajectories $\mathbf{x}(t)$, for which $V[\mathbf{x}(t)] < \infty$, $\forall t$ with probability 1 (see e.g. [19]).

positively correlated two-tag particle histories upon increasing density, mirroring the emergence of collective fluctuations breaking Markovianity in tagged particle motion and leading to tracer subdiffusion. Clear and long-lived deviations of local time statistics from shot-noise behavior demonstrate the insufficiency of harmonization concepts for describing tracer diffusion on a trajectory level. More generally, the connection to the relaxation spectrum provides an intuitive understanding of non-Poissonian statistics at sub-ergodic times in a general setting.

## 2. General theory

We consider a trajectory of a general $N$-dimensional system $\mathbf{x}(t)$ evolving according to Fokker–Planck or discrete-state Markovian dynamics. We are interested in ergodic systems with a unique steady-state $\overline{P}(\mathbf{x})$ and also assume steady state initial conditions. Due to ergodicity the mean local time fraction $\langle\theta_t^j(y)\rangle$ under these conditions is independent of $t$[2] and coincides with the invariant measure $\langle\theta_t^j(y)\rangle = \int \mathrm{d}\mathbf{x}^N\delta(y - x_j)\overline{P}(\mathbf{x})$, where we introduced the Dirac delta function $\delta(x)$ (for a proof see equation (A8)). In the presence of detailed balance (DB) $\overline{P}(\mathbf{x})$ is the Boltzmann–Gibbs measure $P_{\mathrm{eq}}(\mathbf{x})$.

Obtaining equations (2)–(3) essentially amounts to computing the probability generating function of the joint local time functional given by the Feynman–Kac path integral

$$Q_{u,v}(x^i, y^j|t) = \hat{\mathcal{L}}_u^{\vartheta^i}\hat{\mathcal{L}}_v^{\vartheta^j}\langle\delta(\vartheta^i - t\theta_t^i(x))\delta(\vartheta^j - t\theta_t^j(y))\rangle, \tag{4}$$

where we introduced the Laplace transform $\hat{\mathcal{L}}_s^{\vartheta}f(\vartheta) = \int_0^\infty \mathrm{d}\vartheta \mathrm{e}^{-s\vartheta}f(\vartheta)$. The moments in equations (2)–(3) are obtained from $\langle\theta_t^i(x)^n\theta_t^j(y)^m\rangle = t^{-2}\partial_v^n\partial_u^m Q_{u,v}(x^i, y^j|t)|_{u=v=0}$ with $n + m = 2$. A straightforward generalization of the trotterization in [22] shows that $Q_{u,v}(x^i, y^j|t)$ is the propagator of a tilted evolution operator (see appendix A)

$$\begin{aligned} Q_{u,v}(x^i, y^j|t) &= \langle -|\mathrm{e}^{-t(\hat{L}+u\mathbb{1}_x^i+v\mathbb{1}_y^j)}|\mathrm{ss}\rangle \\ &= \langle \mathrm{ss}|\mathrm{e}^{-t(\hat{L}^\dagger+u\mathbb{1}_x^i+v\mathbb{1}_y^j)}|-\rangle, \end{aligned} \tag{5}$$

where $\hat{L}$ and $\hat{L}^\dagger$ denote the 'bare' forward and adjoint (backward) generator of the Markov process [23], and we introduced the 'flat' $|-\rangle \equiv \int \mathrm{d}\mathbf{x}|\mathbf{x}\rangle$ and steady states $|\mathrm{ss}\rangle = \int \mathrm{d}\mathbf{x}\overline{P}(\mathbf{x})|\mathbf{x}\rangle$ in the bra-ket notation, which are the left (right) and right (left) ground eigenstates of $\hat{L}$ ($\hat{L}^\dagger$), respectively. We obtain exact expressions for the moments in equations (2)–(3) by performing a Dyson series-expansion of equation (A3) [24], converging for any bounded functional of $\mathbf{x}(t)$ (see proof in appendix A).

Having assumed diagonalizability of $\hat{L}^\dagger$ (and $\hat{L}$)[3], we expand the backward operator in a complete bi-orthogonal set of left and right eigenstates[4], $\hat{L}^\dagger = \sum_k \lambda_k|\psi_k^L\rangle\langle\psi_k^R|$, $\lambda_k$ denoting the (possibly degenerate) eigenvalues and $\langle\psi_k^L|\psi_l^R\rangle = \delta_{kl}$. The details of the calculation of the moments are shown in appendix A. Obviously, $\langle\psi_0^R|\mathbb{1}_x^i|\psi_0^L\rangle = \overline{P}(x)$, since the system is ergodic. The exact results for the variance and correlations are conceptually remarkably simple and read

$$\sigma_{x_i}^2(t) = \sum_{k\geqslant 1} 2\frac{\Omega_k(x_i, x_i)}{\lambda_k t}\left(1 - \frac{1 - \mathrm{e}^{-\lambda_k t}}{\lambda_k t}\right), \tag{6}$$

$$\mathcal{C}_{xy}^{ij}(t) = \sum_{k\geqslant 1} \frac{\Omega_k(x_i, y_j) + \Omega_k(y_j, x_i)}{\lambda_k t}\left(1 - \frac{1 - \mathrm{e}^{-\lambda_k t}}{\lambda_k t}\right) \tag{7}$$

where we introduced the auxiliary function $\Omega_k(x_i, y_j) \equiv \langle\psi_0^R|\mathbb{1}_x^i|\psi_k^L\rangle\langle\psi_k^R|\mathbb{1}_y^j|\psi_0^L\rangle$. The exact LD limits of equations (6)–(7) readily follow in the limit $t \gg \lambda_1^{-1}$

$$\sigma_{x_i}^{2,\mathrm{LD}}(t) \simeq 2t^{-1}\sum_{k\geqslant 1}\lambda_k^{-1}\Omega_k(x_i, x_i), \tag{8}$$

$$\mathcal{C}_{xy}^{ij,\mathrm{LD}}(t) \simeq t^{-1}\sum_{k\geqslant 1}\lambda_k^{-1}[\Omega_k(x_i, y_j) + \Omega_k(y_j, x_i)], \tag{9}$$

where $\simeq$ denotes asymptotic equality. Analogous formulas for LD limits of local times not connected to a spectral expansion have also been developed (see e.g. [26]). Notably, for systems obeying DB $\sigma_{x_i}^{2,\mathrm{LD}}(t)$ sets a universal upper bound on the variance of $\theta_t$ (compare equations (6) and (8)). The results in equations (6)–(9) readily extend to arbitrary functionals $t^{-1}\int_0^t \hat{V}[\mathbf{x}(\tau)]\mathrm{d}\tau$ with a bounded and local $\hat{V}$, by performing a simple

[2] On the level of the mean alone the time-ordering in the functional in equation (1) is not important (for a proof see equation (A8)).

[3] A sufficient but not necessary condition guaranteeing diagonalizability is that that the operator is normal, i.e. commutes with its adjoint, $\hat{L}^\dagger\hat{L} - \hat{L}\hat{L}^\dagger = 0$.

[4] Note that $\hat{L}|\psi_k^R\rangle = \lambda_k|\psi_k^R\rangle$ and $\hat{L}^\dagger|\psi_k^L\rangle = \lambda_k|\psi_k^L\rangle$ [25].

exchange $\mathbb{1}^i_x \to \hat{V}$, modifying only $\Omega_k(x_i, y_j)$ (see appendix A). Equations (6)–(7) with the aforementioned generalizations apply to all diagonalizable $\hat{L}$, thus including all systems obeying DB, and represent our first main result.

Equations (6)–(9) provide an intuitive understanding of local time statistics via a mapping onto relaxation eigenmodes, with fluctuation and correlation amplitudes proportional to the sum of transition amplitudes of excitations from the steady state to excited states and back, $\Omega_k(x_i, y_j)$. On ergodic time scales $\theta_t$ at different $t$ decorrelate, and hence display features of shot-noise, i.e. $\sigma^2_{x_i}(t)$ and $\mathcal{C}^{ij}_{xy}(t)$ decay inversely proportional to the number of independent observations of each excitation mode, $\sim\lambda_k^{-1}/t$. At finite times $t \lesssim \lambda_k^{-1}$ shot-noise statistics are altered due to a finite survival probability of the eigenmodes at a given $t$, $(1 - \mathrm{e}^{-\lambda_k t})/\lambda_k\ \forall k$, setting a hierarchy of correlation times $\lambda_k^{-1}$ (see correction terms in brackets of equations (6)–(7)).

## 3. Local times in single-file diffusion

Consider the dynamics of $N$ identical hard-core interacting Brownian point particles diffusing in the unit interval $[0,\ 1]$, and set $D = 1$ without loss of generality. The extension to a finite particle radius follows from a trivial change of coordinates [8]. Let $P(\mathbf{x}_0,\ t|\mathbf{x}) \equiv \langle \mathbf{x}_0|\mathrm{e}^{-t\hat{L}^\dagger}|\mathbf{x}\rangle$ denote the $N$-particle backward propagator of the single file with the following backward generator and $N - 1$ internal non-crossing boundary conditions:

$$\hat{L}^\dagger = -\sum_{i=1}^{N}\partial^2_{x_i}, \qquad \lim_{x_{i+1}\to x_i}(\partial_{x_{0,i+1}} - \partial_{x_{0,i}})P(\mathbf{x}_0,\ t|\mathbf{x}) = 0 \quad \forall i. \tag{10}$$

Confinement into a unit interval is imposed through external reflecting boundary conditions $\partial_{x_1}P(\mathbf{x}_0,\ t|\mathbf{x})|_{x_{0,1}=0} = \partial_{x_N}P(\mathbf{x},\ t|\mathbf{x}_0)|_{x_{0,N}=1} = 0$. Under these boundary conditions we diagonalize $\hat{L}^\dagger$ using the coordinate Bethe ansatz [27][5] and obtain the Bethe eigenvalues $\lambda_k = \pi^2\sum_i k_i^2$ and corresponding left and right eigenvectors

$$\psi^L_k(\mathbf{x}) \equiv \langle \mathbf{x}|\psi^L_k\rangle = {\sum_{\{k_i\}}}'\prod_{i=1}^{N} 2^{(1-\delta_{k_i,0})/2}\cos(k_i\pi x_i) \tag{11}$$

and $\psi^R_k(\mathbf{x}) \equiv \langle \psi^R_k|\mathbf{x}\rangle = m_k\psi^L_k(\mathbf{x})$ with $\langle\psi^R_k|\psi^L_l\rangle = \delta_{k,l}$, where $m_k$ is the multiplicity of the Bethe eigenmode $|\psi^L_k\rangle$ (see appendix C), and ${\sum_{\{k_i\}}}'$ denotes the sum over all permutations of single-particle eigenvalues with $k_i \in \mathbb{N}_0$.

The matrix elements entering $\Omega_k(x_i, y_j)$ follow upon integration over the $n_l$ and $n_r$ particle coordinates to the left and right, respectively, from the tagged particle $i$ while strictly preserving the particle ordering [8], yielding (see appendix B) $\langle\psi^R_k|\mathbb{1}^i_x|\psi^L_0\rangle = \frac{N!}{m_k}\langle\psi^R_0|\mathbb{1}^i_x|\psi^L_k\rangle$ with

$$\langle\psi^R_0|\mathbb{1}^i_x|\psi^L_k\rangle = \frac{m_k}{n_l!n_r!}{\sum_{\{k_i\}}}'{}^{1}_{x}\Lambda^c_i\prod_{j=1}^{i-1}{}^{x}_{x}\Lambda^s_j\prod_{k=i+1}^{N}{}^{1-x}_{x}\Lambda^s_k, \tag{12}$$

and $\langle\psi^R_k|\mathbb{1}^i_x|\psi^L_0\rangle = \frac{N!}{m_k}\langle\psi^R_0|\mathbb{1}^i_x|\psi^L_k\rangle$. In equation (12) we have defined the auxiliary functions

$$\begin{aligned}{}^{y}_{x}\Lambda^c_i &= y\delta_{k_i,0} - (1 - \delta_{k_i,0})\sqrt{2}\cos(\pi k_i x)\\ {}^{y}_{x}\Lambda^s_i &= y\delta_{k_i,0} - (1 - \delta_{k_i,0})\sqrt{2}\sin(\pi k_i x)/\pi k_i.\end{aligned} \tag{13}$$

This delivers exact results for $\sigma^2_{x_i}(t)$ and $\mathcal{C}^{ij}_{xy}(t)$ in equations (6)–(8). An efficient numerical implementation of our analytical results can be made available upon request.

The results for $\sigma^2_{x_i}(t)$ in equation (6) for the central particle in single files with various $N$ are depicted in figure 2, and reflect large fluctuations exceeding 200% on time-scales where roughly only 50% of the particles have collided with their neighbors. The fluctuations display a non-trivial dependence on $x$, which does not follow the shape of $P_{\mathrm{eq}}(x_t) = N!x_t^{n_l}(1 - x_t)^{n_r}/(n_l!n_r!)$, and reveal striking boundary-layer effects. These deviations are clear evidence for non-Poissonian statistics and signal that harmonization concepts, which assume a locally equilibrated environment [14], break down on the more fundamental trajectory level. At longer $t$, where ~50–100 collisions/particle have occured, $\theta^i_t$ at different $t$ become uncorrelated according to the central limit theorem, with $\sigma^2_{x_c}(t)$ converging to its LD limit (8). On these time-scales the ensemble MSD has already saturated (compare figures 1(a) and 2(c) and (d)). Notably, LD asymptotics correctly capture only small fluctuations of the order $\pm 10\%$. As noted above and confirmed by simulations, LDs reflecting Gaussian statistics set an upper bound to the fluctuations of $\theta^i_t$ (figures 2(c) and (d)).

Single-file diffusion displays no time-scale separation in the relaxation spectrum. As a result, the projection of dynamics onto a tagged particle coordinate induces subdiffusion and strong non-Markovianity on time scales $t < \lambda_1^{-1}$. The respective onset of the $\sqrt{t}$ scaling of the tagged particle MSD shifts to shorter $t$ upon increasing $N$

[5] Note the difference with respect to the momentum-space Bethe ansatz solution [8], which does not diagonalize $\hat{L}$.

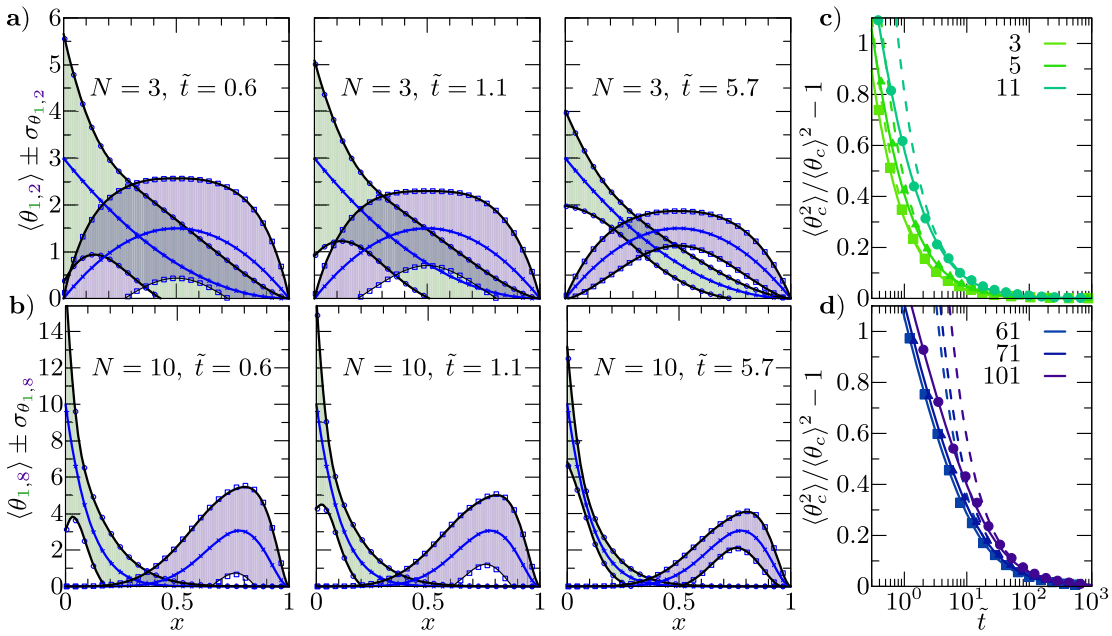


**Figure 2.** Statistics of local time fraction: mean, $\langle\theta_t^i(x)\rangle$, (blue lines) and fluctuations reflected by the shaded area enclosed by black lines corresponding to $\langle\theta_t^i(x)\rangle \pm \sigma_{x_i}(t)$ for (a) the first (green) and second (violet), and (b) first (green) and 8th (violet) tagged particle in a single file with $N = 3$ and $N = 10$, respectively at three different lengths of trajectories. The black lines correspond to 'error bars' on a finite-time estimate of the probability density along a single trajectory starting in the steady-state. (c) and (d): reduced variance of local time of the central particle $\sigma^2_{x_c=1/2}(t)\big/\langle\theta_t^c(x_c = 1/2)\rangle^2$ for various odd $N$ in order to preserve the symmetry. The full lines denote exact results from equation (6) and dashed lines large deviation asymptotics equation (8). Symbols correspond to Brownian dynamics simulation of an ensemble of $10^6$ independent trajectories starting from equilibrium initial conditions.

(figure 1(a)). Increasing $N$ in turn leads to a high degeneracy of Bethe eigenmodes, reflecting emerging dynamical symmetries (see appendix F). As a result, fewer Bethe modes are required for a convergence of the sums in equations (6)–(7).

To gain deeper insight into the physical origin of the memory on a trajectory level we analyzed two-tag correlations between particle histories by means of the reduced covariance of local times $\tilde{\mathcal{C}}^{ij}_{xy}(t) = \mathcal{C}^{ij}_{xy}(t)\big/(\langle\theta_t^i(x)\rangle\langle\theta_t^j(y)\rangle)$, with $\tilde{\mathcal{C}}^{ij}_{xy}(t) \in [-1, \infty)$. Correlations between the histories of the central particle $c$ and its nearest (i.e. $c + 1$) and next-nearest (i.e. $c + 2$) neighbors at the midpoint between the maxima of $P_{\rm eq}(x_c)$ and $P_{\rm eq}(x_{c+1,c+2})$ (see appendix E and H for details) are depicted in figure 3. Due to ergodicity, $\theta_t^i(x)$ become very weakly correlated at long $t$ and Gaussian statistics emerge. Consequently, $\tilde{\mathcal{C}}^{ij}_{xy}(t)$ vanishes for long times, after $\gtrsim 10^2$ collisions took place on average. Note that $\mathcal{C}^{ij}_{xy}(t)$ measures correlations between particle histories and not particle positions. The latter never decorrelate, i.e. two-tag position correlation functions display an algebraic decay even at equilibrium $P^{ij}_{\rm eq}(x_i, x_j) = N!x_i^{n_l}(x_j - x_i)^{m_l - n_l}(1 - x_j)^{m_r}\big/(n_l!m_r!(m_l - n_l)!) - P_{\rm eq}(x_i)P_{\rm eq}(x_j) \neq 0$, where $n_{l,r}$ and $m_{l,r}$ are the number of particles to the left/right of the two tagged particles $i$ and $j$ (for details see appendix G).

Notably, we observe a transition from negatively to positively correlated tagged particle histories upon increasing density (figure 3), mirroring a change in particle dynamics from single-particle to collective fluctuations. The driving force for this transition can be found in an enhanced packing at higher densities resembling a 'crystallization' transition, where invariant tagged particle densities $P_{\rm eq}(x)$ become strongly overlapping, whereas their respective widths shrink only very slowly (see figure D1). The 'critical' density, at which the behavior shifts from negatively to positively correlated histories, depends on the topological separation between the two tagged particles and is shifted to higher values of $N$ for more distant particles (compare (a) and (b) in figure 3). In turn, this reflects a growing dynamical correlation-length with increasing $N$. As the mathematical reason for the sign-change are different signs of leading eigenvectors entering the respective elements (see equation (12)), the transition will eventually occur of any tagged pair. Moreover, upon increasing $N$, $\tilde{\mathcal{C}}^{ii}_{xy}(t)$ of the central particle becomes non-monotonic, with weak anti-correlations at short $t$ turning to weak correlations at large $t$, before reaching the LD limit of uncorrelated histories, where harmonization [14] ideas apply. The increasingly positive correlations with growing $N$ reflect a persistence and a finite life-time of typical collective fluctuations on a trajectory level, akin to glassy dynamics in kinetically constrained models [28]. Accordingly, positive correlations are are not observed if we tag outer particles at external boundaries (see appendix H). The exact results for fluctuations and correlations of local times in single file diffusion in

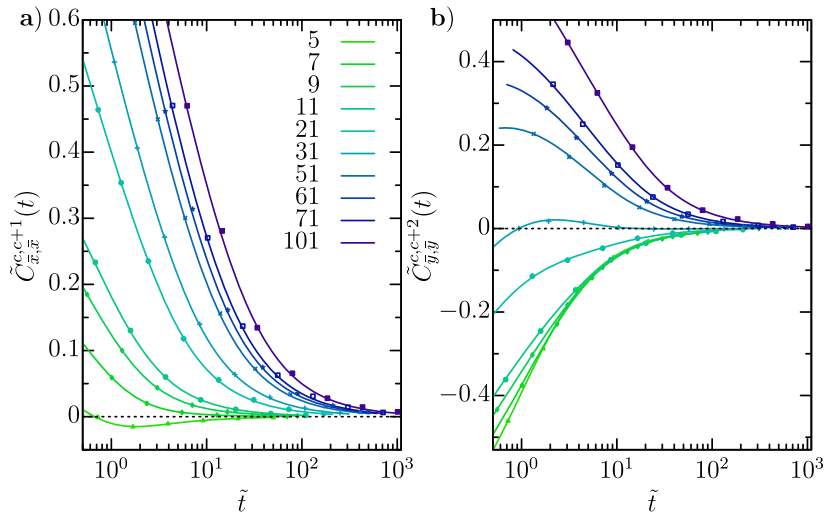


**Figure 3.** $\tilde{\mathcal{C}}^{ij}_{xy}(t) = \mathcal{C}^{ij}_{xy}(t)\big/(\langle\theta^i_t(x)\rangle\langle\theta^j_t(y)\rangle)$, reduced two-tag local time correlation functions of the central particle $c$ and its nearest (a) and next-nearest (b) neighbor for different $N$. Only odd $N$ were considered to assure the symmetry required for a meaningful comparison. Time is expressed in units of the mean collision time. Lines depict the theory in equation (7) whereas symbols correspond to Brownian dynamics simulations of $10^6$ independent trajectories starting from equilibrium initial conditions.

equations (11)–(13), and the explanation of the origin of broken Markovianity on a trajectory level are our second main result.

## 4. Conclusions

We established a general method for determining exactly the variance and two-tag correlations of bounded non-negative functionals of stationary ergodic Markov processes with a diagonalizable propagator. The theory relates the statistics of functionals to the relaxation eigenspectrum, and allows for an exact treatment of non-Markovian dynamics from the corresponding higher-dimensional Markovian embedding. It also holds for diagonalizable irreversible dynamics, where a broken time-reversal symmetry can cause oscillations in higher order terms in equations (6)–(9) and/or fluctuations exceeding the LD limit in equation (8). From the spectrum of the many-body propagator obtained via the coordinate Bethe ansatz, we derived exact results for one- and two-tag local times in single file diffusion, which unveiled non-trivial correlations between tagged particle histories and the emergence of collective dynamics at increasing particle densities. Going beyond LD time-scales, our results revealed that harmonization concepts, assuming dynamics in-between local equilibria—an assumption that works well for ensemble-average observables [14]—fail on the more fundamental trajectory level. This highlights the intricate physical meaning of projection-induced memory on the level of single trajectories, which is virtually invisible to ensemble-average observables. Our results on local times can be readily tested by existing particle-tracking experiments (see e.g. [5]), and hopefully our theory will stimulate further research directed towards tagged particle functionals. Particularly interesting would be extensions to tagged particle dynamics in rugged potential landscapes [29].

## Acknowledgments

We thank David Hartich for insightful discussions and critical reading of the manuscript. The financial support from the German Research Foundation (DFG) through the *Emmy Noether Program 'GO 2762/1-1'* (to AG), and an IMPRS fellowship of the Max Planck Society (to AL) are gratefully acknowledged.

## Appendix A. Proof of the main result

Let $\mathbf{x}(t)$ be an arbitrary-dimensional ergodic Markov process on a discrete or continuous state-space. The evolution of the probability density function evolves under the corresponding *diagonalizable* forward generator $\hat{L}$ (e.g. Fokker–Planck- or discrete-state master equation-type) with invariant measure $\overline{P}(\mathbf{x})$ and the adjoint (i.e. backward) generator $\hat{L}^\dagger$. Let the respective eigenspectra be $\hat{L} = \sum_k \lambda_k |\psi^R_k\rangle\langle\psi^L_k|$, $\lambda_k$ and $\hat{L}^\dagger = \sum_k \lambda_k |\psi^L_k\rangle\langle\psi^R_k|$, $\lambda_k$ denoting the possibly degenerate and in general complex-valued eigenvalues. Note that $\hat{L}|\psi^R_k\rangle = \lambda_k|\psi^R_k\rangle$ and

$\hat{L}^\dagger|\psi_k^L\rangle = \lambda_k|\psi_k^L\rangle$, i.e. the left and right eigenstates span a bi-orthogonal eigenspace $\langle\psi_k^L|\psi_l^R\rangle = \delta_{kl}$ [25]. The forward and backward propagators of the process can then be written as [25]

$$P_{\rm f}(\mathbf{x},\,t|\mathbf{x}_0) = \langle\mathbf{x}|e^{-t\hat{L}}|\mathbf{x}_0\rangle = \sum_k \langle\mathbf{x}|\psi_k^R\rangle\langle\psi_k^L|\mathbf{x}_0\rangle e^{-\lambda_k t}$$
$$P_{\rm b}(\mathbf{x},\,t|\mathbf{x}_0) = \langle\mathbf{x}_0|e^{-t\hat{L}^\dagger}|\mathbf{x}\rangle = \sum_k \langle\mathbf{x}_0|\psi_k^L\rangle\langle\psi_k^R|\mathbf{x}\rangle e^{-\lambda_k t}. \tag{A1}$$

Obviously, for $\hat{L}$ with a partially continuous spectrum[6] the sum would be replaced by the corresponding integral, the probability density function of a bounded functional $\varphi_t = \int_0^t \hat{V}[\mathbf{x}(\tau)]\,d\tau$ over all paths starting from a (potentially non-equlibrium) steady-state and propagating up to time $t$, is defined by the path integral

$$\mathcal{F}(\varphi|t) = \int\int d\mathbf{x}d\mathbf{x}_0\overline{P}(\mathbf{x}_0)\int_{\mathbf{x}(0)=\mathbf{x}_0}^{\mathbf{x}(t)=\mathbf{x}}\mathscr{D}[\mathbf{x}(t)]e^{-\mathcal{S}[\mathbf{x}(t)]}\delta(\varphi - \int_0^t \hat{V}[\mathbf{x}(\tau)]\,d\tau), \tag{A2}$$

with the corresponding stochastic action functional $\mathcal{S}[\mathbf{x}(t)]$ of the continuous [22, 30] or discrete state-space [31] Markov process $\mathbf{x}(t)$, and where we introduced the Dirac delta function $\delta(x)$. By means of a straightforward vectorial generalization of the trotterization of the the path integral (A2) in [19, 22] (for the backward and forward approach, respectively), one finds that the generating function, corresponding to the Laplace transform $\tilde{\mathcal{F}}(u|t) = \int_0^\infty d\varphi e^{-u\varphi}\mathcal{F}(\varphi|t)$, is the propagator of a tilted operator

$$\tilde{\mathcal{F}}(u|t) = \langle -|e^{-t(\hat{L}+u\hat{V})}|\mathrm{ss}\rangle = \langle \mathrm{ss}|e^{-t(\hat{L}^\dagger+u\hat{V})}|-\rangle, \tag{A3}$$

where we have introduced the 'flat' $|-\rangle \equiv \int d\mathbf{x}|\mathbf{x}\rangle$ and steady states $|\mathrm{ss}\rangle = \int d\mathbf{x}\overline{P}(\mathbf{x})|\mathbf{x}\rangle$, which are the left (right) and right (left) ground eigenstates of $\hat{L}$ ($\hat{L}^\dagger$), respectively. The last equality follows from $\tilde{\mathcal{F}}(u^\dagger|t)^\dagger = \tilde{\mathcal{F}}(u|t)$. In taking the Laplace transform we assumed that the functional has non-negative support (such as in the case of local times). In case the support extends to negative values one simply needs to take the Fourier transform instead.

The moments of $\mathcal{F}(\varphi|t)$ at any given $t$ follow immediately from $\langle\varphi_t^n\rangle = (-1)^n\partial_u^n\tilde{\mathcal{F}}(u|t)|_{u=0}$, where $\langle\cdots\rangle$ denotes the average over all trajectories starting from a steady state and propagating up to time $t$. In case the Fourier transform is used, a corresponding change of the prefactor is required.

For bounded functionals of ergodic Markov processes all moments are finite, $|\langle\varphi_t^n\rangle| \leqslant f(t)\lim_{t\to\infty}|\langle\varphi_t^n\rangle| < \infty$ with a smooth scaling function $f(t)$, which depends on the detailed form of $\hat{V}[\mathbf{x}(t)]$. This follows from the fact that the integral is always over a finite time (see e.g. equation (1)) and hence boundedness of the integrand assures the boundedness of the time-average observable. Moreover, $\mathcal{F}(\varphi|t)$ obeys a LD principle [18, 32]. In the specific case of local times, $\hat{V}[\mathbf{x}(t)] = \mathbb{1}_y^j[\mathbf{x}(t)]$ and $f(t) \propto t^n$ for $\langle\varphi_t^n\rangle$. The finiteness of moments implies that $\tilde{\mathcal{F}}(u|t)$ is an analytic (i.e. holomorphic) function of $u$ at least at and near $u = 0$ for any $t$.

Note that for bounded $\hat{V}[\mathbf{x}(t)]$ we can always write

$$\int_0^t dt'\hat{V}[\mathbf{x}(t')] = \int_0^t dt'\int d\mathbf{x}\delta(\mathbf{x} - \mathbf{x}(t'))V(\mathbf{x})$$
$$= \int d\mathbf{x}V(x)\int_0^t dt'\delta(\mathbf{x} - \mathbf{x}(t')) \equiv t\int d\mathbf{x}V(\mathbf{x})\theta_t(\mathbf{x}). \tag{A4}$$

To obtain exact results for second moments we simply need to expand $\tilde{\mathcal{F}}(u|t)$ in a Dyson series to second order in $u\hat{V}$ preserving the time-ordering, and afterwards take the second derivative at $u = 0$. The series is guaranteed to converge, since $\hat{V}$ is bounded. Because trivially $\langle -|e^{-t\hat{L}}|\mathrm{ss}\rangle = \langle \mathrm{ss}|e^{-t\hat{L}^\dagger}|-\rangle = 1$, the Dyson expansion gives [24]

$$\langle \mathrm{ss}|e^{-t(\hat{L}^\dagger+u\hat{V})}|-\rangle = 1 - u\langle \mathrm{ss}|\int_0^t dt' e^{-\hat{L}^\dagger(t-t')}\hat{V}e^{-\hat{L}^\dagger t'}|-\rangle$$
$$+ u^2\langle \mathrm{ss}|\int_0^t dt'\int_0^{t'} dt'' e^{-\hat{L}^\dagger(t-t')}\hat{V}e^{-\hat{L}^\dagger(t'-t'')}\hat{V}e^{-\hat{L}^\dagger t''}|-\rangle + \mathcal{O}(u^3), \tag{A5}$$

with $t \geqslant t' \geqslant t'' \geqslant 0$. An equivalent expansion can be obtained for $\hat{L}$. The Dyson series (A5) converges for $u \in \mathbb{C} < \infty$.

We first prove the convergence for any bounded *linear* operator $\hat{B}$. To this end we consider the operator norm. Let $\Psi$ be a complete normed linear space, and $\hat{B} : \Psi \to \Psi$. The operator norm is then defined as $||\hat{B}|| = \sup_{||\psi||=1}||\hat{B}\psi||$ with $\psi \in \Psi$. The operator norm corresponds to the largest value $\hat{B}$ stretches an element of $\Psi$. Since $\hat{B}$ is bounded we have $||\hat{B}^N|| \leqslant ||\hat{B}||^N$, $\forall N \in \mathbb{N}$, which follows simply from $||\hat{A}\hat{B}|| \leqslant ||\hat{A}||\,||\hat{B}||$. The operator exponential is defined as the limit $e^{\hat{B}} = \lim_{N\to\infty}\sum_{k=0}^N \hat{B}^k/k!$ and the convergence is in operator norm, since $||\sum_{k=0}^N \hat{B}^k/k!|| \leqslant \sum_{k=0}^N||\hat{B}||^k/k!$, $\forall N \in \mathbb{N}$. The series on the right hand side converges absolutely for any number $||\hat{B}|| \in \mathbb{C}$. Due to the completeness of the space $\Psi$, $e^{\hat{B}}$ as well belongs to a complete normed linear space, and moreover $||e^{\hat{B}}|| \leqslant e^{||\hat{B}||}$. Taking $\hat{B} = u\hat{V}$ with $u \in \mathbb{C}$ completes the proof of convergence of the series (A5).

[6] The ground state is always discrete as we assume the existence of an invariant measure.

We now show that the following results also hold for *bounded nonlinear functionals* $\hat{V}$ such that the two-term Dyson expansion in equation (A5) is always well-behaved. Utilizing the identities in equation (A4) we find that

$$\langle V\rangle = t\int \mathrm{d}\mathbf{x} V(\mathbf{x})\langle\theta_t(\mathbf{x})\rangle, \tag{A6}$$

$$\langle V^2\rangle = t^2\int \mathrm{d}\mathbf{x}\int \mathrm{d}\mathbf{x}' V(\mathbf{x})V(\mathbf{x}')\langle\theta_t(\mathbf{x})\theta_t(\mathbf{x}')\rangle. \tag{A7}$$

Since both $\langle\theta_t(\mathbf{x})\rangle$ and $\langle\theta_t(\mathbf{x})\theta_t(\mathbf{x}')\rangle$ are strictly bounded, $\langle V\rangle$ and $\langle V^2\rangle$ are also bounded, because $\hat{V}[\mathbf{x}(t)]$ is by definition bounded. For bounded $\hat{V}$ (linear or nonlinear) this proves that at least the two-term Dyson expansion is thus always finite and well behaved (in fact all orders are a.s.).

Utilizing now the spectral expansion $\hat{L}^\dagger = \sum_k \lambda_k|\psi_k^L\rangle\langle\psi_k^R|$ in equation (A5) we obtain for the first order term

$$\int_0^t \mathrm{d}t'\langle \mathrm{ss}|\sum_k|\psi_k^L\rangle\langle\psi_k^R|\mathrm{e}^{-\lambda_k(t-t')}\hat{V}\sum_l|\psi_l^L\rangle\langle\psi_l^R|\mathrm{e}^{-\lambda_l t'}|-\rangle = tV_{00}, \tag{A8}$$

where we introduced $V_{lk} = \langle\psi_l^R|\hat{V}|\psi_k^L\rangle$ and we used the fact that $\langle\mathrm{ss}|$ and $|-\rangle$ are the left and right ground states of $\hat{L}^\dagger$ as well as the bi-orthogonality of the eigenbasis. The second order term follows similarly

$$\int_0^t\mathrm{d}t'\int_0^{t'}\mathrm{d}t''\sum_l V_{l0}V_{0l}\mathrm{e}^{-\lambda_l(t'-t'')} = \frac{V_{00}^2t^2}{2} + t^2\sum_{l\neq 0}\frac{V_{l0}V_{0l}}{\lambda_l t}\left(1-\frac{1-\mathrm{e}^{-\lambda_l t}}{\lambda_l t}\right). \tag{A9}$$

We can now trivially extend $u\hat{V}\to u\hat{A}+v\hat{B}$ for $u,\,v\in\mathbb{C}$ and any two bounded operators $\hat{A}$ and $\hat{B}$. In the specific case of tagged particle local times studied in the main text we have $\hat{A} = \mathbb{1}_y^j[\mathbf{x}(t)]$ and $\hat{B} = \mathbb{1}_z^j[\mathbf{x}(t)]$, where $\mathbb{1}_y^j[\mathbf{x}(\tau)] = 1$ if $x_j\in\mathrm{d}y$ centered at $y$, and zero otherwise [18]. The exact second moments are now obtained from $\partial_u\partial_v\tilde{\mathcal{F}}(u|t)|_{u=v=0}$ and $\partial_u^2\tilde{\mathcal{F}}(u|t)|_{u=0}$ by considering the corresponding operators $\hat{A}$ and $\hat{B}$.

Finally, since we consider the local time fraction and not the total local time, we must take $t^{-2}\partial_u\partial_v\tilde{\mathcal{F}}(u|t)|_{u=v=0}$ and $t^{-2}\partial_u^2\tilde{\mathcal{F}}(u|t)|_{u=0}$, respectively. This completes the proof of the main general results, i.e. equations (6) and (7).

## Appendix B. Extended phase-space integration in single-file diffusion

The integrals involved in the evaluation of invariant measures and matrix elements in single-file diffusion involve nesting, i.e. the ordering of particles is strictly preserved

$$\int_a^{\not b} f(\mathbf{x})\mathrm{d}\mathbf{x} = \int_a^b \mathrm{d}x_1\int_{x_1}^b \mathrm{d}x_2\cdots\int_{x_{N-2}}^b \mathrm{d}x_{N-1}\int_{x_{N-1}}^b \mathrm{d}x_N f(\mathbf{x}). \tag{B1}$$

This imposes non-trivial topology of the phase space of the system. A tremendous simplification is achieved through the so-called 'Extended Phase-Space Integration' developed by Lizana and Ambjörnsson, which exactly reduces the nested high-dimensional integrals to scaled single particle integrals, e.g. [8]:

$$\int_a^{\not b} f(\mathbf{x})\delta(x_\mathrm{m}-z)\mathrm{d}\mathbf{x} = \left(\prod_{i=1}^{m-1}\int_a^z \mathrm{d}x_i\right)\left(\prod_{j=m+1}^{N}\int_z^b \mathrm{d}x_j\right)\frac{f(x_m=z,\,\mathbf{x}_{N-1})}{n_l!n_r!}, \tag{B2}$$

where $n_l$ and $n_r$ are the number of particles (integrals) to the left and right of the tagged particle $m$, respectively. The extended phase-space integration in equation (B2) applies to all functions $f(\mathbf{x})$, which are invariant under the exchange $x_i\leftrightarrow x_{i+1}$. Throughout our work all nested integrals included in the bra-s $\langle\psi_k|$ (scalar products, matrix elements etc) are evaluated using the extended phase-space integration.

## Appendix C. Eigenmode multiplicity and eigenvalue degeneracy

As described in the main text we diagonalize the many-body Fokker–Planck operator using the coordinate Bethe ansatz method. Each Bethe eigenstate of a Single-File of $N$ particles is uniquely defined by a tuple $k = (k_1, k_2, \ldots, k_N)$. To each tuple corresponds one eigenvalue through the relation:

$$\lambda_k = \sum_{i=1}^N \pi^2 k_i^2 \tag{C1}$$

since more than one tuple may correspond to the same eigenvalue, these are degenerate. To each tuple $k$ it is possible to associate a set $\mathcal{K}$ containing the elements of $k$ counted once. Defining $n_{\mathcal{K}_i}$ as the number of times the element $\mathcal{K}_i$ appears in the tuple $k$, we define the multiplicity of the eigenvectors associated to $k$ as

$$m_k = \prod_i n_{\mathcal{K}_i}!. \tag{C2}$$

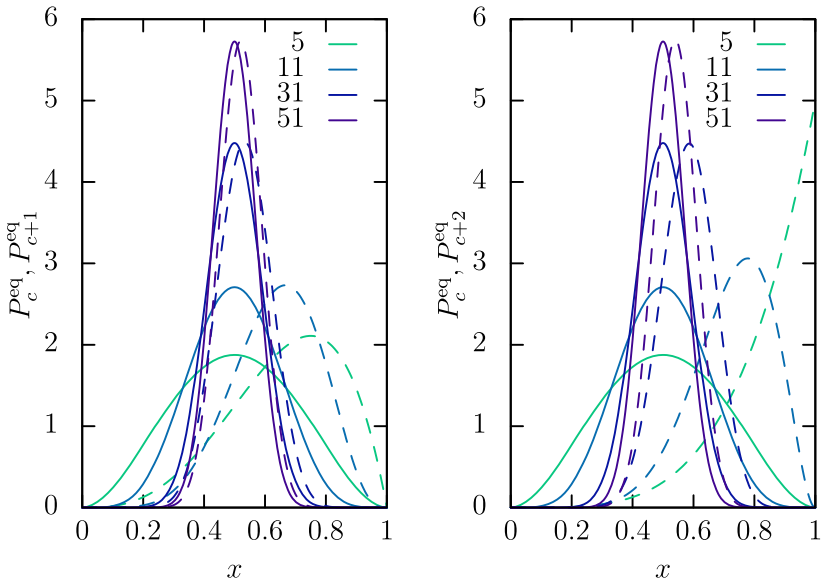


**Figure D1.** The solid lines represent the equilibrium probability density (D1) of the central particle and the dashed lines of the right nearest neighbor (left) and the next-nearest neighbor (right), respectively.

## Appendix D. Tagged particle equilibrium probability densities

The exact tagged particle equilibrium probability density function of the tagged particle $i$ is obtained by a nested integration of all other particle positions

$$P_i^{\rm eq}(x) = \int_0^1 P_{\rm eq}(\mathbf{x})\,\delta(x_i - x)\,{\rm d}\mathbf{x} = \frac{N!}{n_l!n_r!}x^{n_l}(1-x)^{n_r}, \tag{D1}$$

where $n_l$ and $n_r$ are, respectively, the number of particles to the left and to the right of the tagged particle $i$. Figure D1 depicts results for $P_i^{\rm eq}(x)$ for the central particle $c$ and the two nearest neighbors to the right, $c+1$ and $c+2$, respectively. The probability density of the central particle approaches a Gaussian shape as the number density $N$ increases. For large enough $N$ the width of $P_i^{\rm eq}(x)$ stops decreasing appreciably, while the probability densities of neighboring particles begin to overlap strongly. This has important physical consequences for correlations of particle histories, as we explained in the discussion of figure 3 in the main text.

## Appendix E. Reference points in the study of the density dependence of tagged particle local time statistics

In order to allow for a meaningful comparison of results for different particle numbers $N$ we need to choose appropriate reference conditions. To do so, we focus only on odd particle numbers, for which the system is symmetric with respect to the peak of the invariant measure of the central particle $P_{\rm eq}(x_c)$. This way a comparison of correlations with nearest $c+1$ and next-nearest $c+2$ neighbors at different densities is indeed consistent. Moreover, in order to compare equilibrium and near-equilibrium tagged particle excursions with far-from equilibrium fluctuations we choose the following reference points with respect to $P_{\rm eq}(x_i)$: the point $x_{50}$, in which $\int_0^{x_{50}} P_{\rm eq}(x_i)\,{\rm d}x_i = 0.5$, point $x_{75}$, where $\int_0^{x_{75}} P_{\rm eq}(x_i)\,{\rm d}x_i = 0.75$, and point $x_{90}$, for which

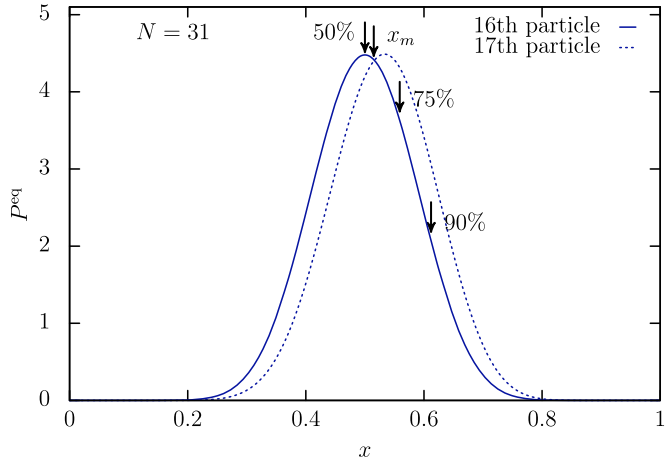


**Figure E1.** Invariant measures for the central particle and its nearest neighbor, denoting the different kinds of reference points.

$\int_0^{x_{90}} P_{eq}(x_i)\mathrm{d}x_i = 0.9$ (see also figure E1). In the study of correlations of particle histories for two particles $i$ and $j$ we focus on the mid-point $x_m(i, j) = (x_{50,i} + x_{50,j})/2$.

## Appendix F. Convergence rates of series and eigenvalue degeneracy

The exact expressions for variance and covariance of local time of a tagged particles in equations (6) and (7) in the main text involve an infinite series, whose rate of convergence is difficult to predict, as it strongly depends on the particular position $x$ of the tagged particle under inspection, as well as on the number of particles $N$ and $\mathcal{D}(k)$, the degeneracy of Bethe eigenvalue $\lambda_k$. To inspect the rate of convergence of the series we compute the relative deviation of the results for the variance of local time of the central particle truncated at the $k$th Bethe eigenvalue, $|\sigma^2_{x_c}(t) - \sigma^2_k(t)|/\sigma^2(t)$ as a function of $k$ at different positions $x$ and at different lengths of trajectories $t$. Figure F1 depicts how fast the series for the variance of local time of the central particle (equation (6) in the main text) truncated at the $k$th term converges to the exact value $k \to \infty$. n order to compare systems with different $N$ we focused on points $x_{50}$ and $x_{75}$ of the central particle, with the specific values given in table F1.

Intuitively, the convergence rate increases with increasing length of the observation $t$, since faster modes must become less and less important. The convergence rate also increases with increasing $N$, which is due to an increasing degeneracy of lower-lying eigenvalues at larger $N$. Degenerate low-lying eigenvalues allow for a mixing of different collective slow modes, which become dominant. Finally, by comparing the columns of figure F1 we notice that the rate of convergence also depends on the tagging position, which in turn depends on the curvature of the modes at different $N$.

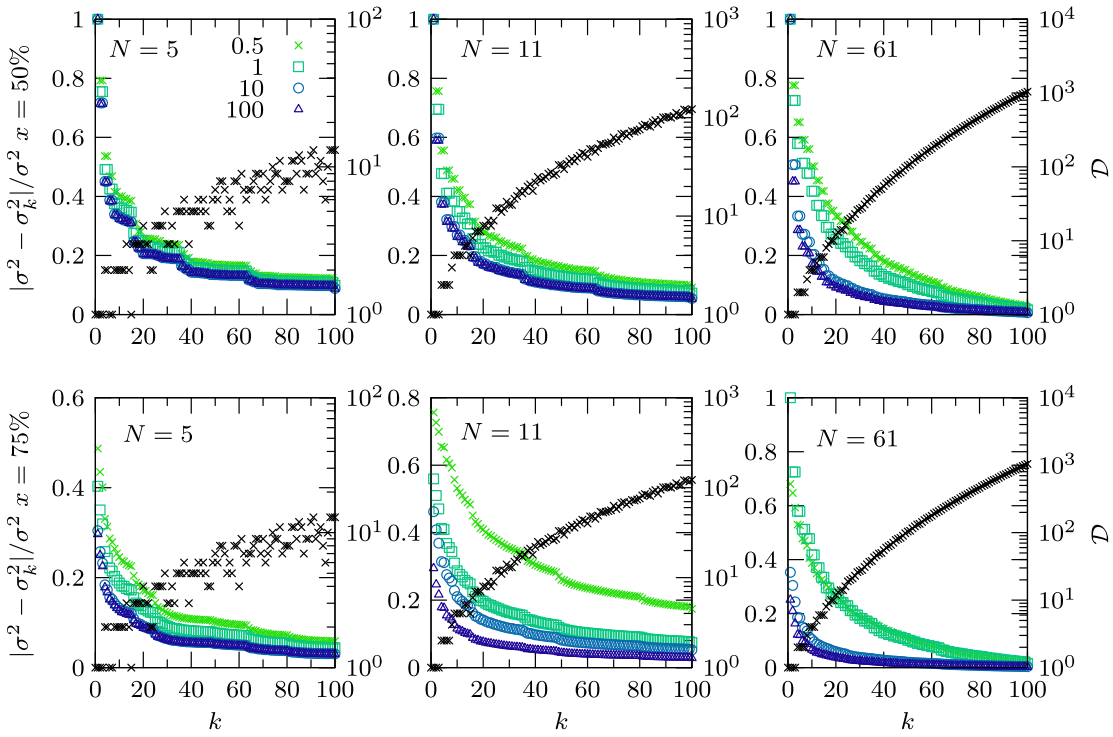


**Figure F1.** Analytical results for $|\sigma^2_{x_c}(t) - \sigma^2_k(t)|/\sigma^2(t)$ of the central particle for different particle numbers ($N$) as a function of $k$ at different tagging positions. The black symbols depict the eigenvalue degeneracy $\mathcal{D}(k)$.

**Table F1.** Location of $x_{50}$ and $x_{75}$ for the central particle for various values of $N$.

| $N$ | $x_{50}$ | $x_{75}$ |
|---|---|---|
| 5 | 0.500 | 0.641 |
| 11 | 0.500 | 0.598 |
| 61 | 0.500 | 0.544 |

## Appendix G. Equilibrium position correlation function

In the main text we focused on the covariance of tagged particle local times $\tilde{C}^{ij}_{xy}(t) = \dfrac{\tilde{C}^{ij}_{xy}(t)}{\langle\theta^i_t(x)\rangle\langle\theta^j_t(y)\rangle}$ reflecting the correlations between particle histories. We found that histories decorrelate at long times as a consequence of the central limit theorem. Conversely, the particle positions on the ensemble average level do not decorrelate, not even in equilibrium. To demonstrate this we compute exactly the pair correlation function

$$\begin{aligned} P^{ij}_{\rm eq}(x_i, x_j) &= \int_0^1 P_{\rm eq}(\mathbf{x})\delta(x_i - x)\delta(x_j - y)\mathrm{d}\mathbf{x} - \int_0^1 P_{\rm eq}(\mathbf{x})\delta(x_i - x)\mathrm{d}\mathbf{x}\int_0^1 P_{\rm eq}(\mathbf{x})\delta(x_j - y)\mathrm{d}\mathbf{x} \\ &= \frac{N! x_i^{n_l}(x_j - x_i)^{m_l - n_l}(1 - x_j)^{m_r}}{n_l! m_r!(m_l - n_l)!} - \frac{(N!)^2 x_i^{n_l}(1 - x_i)^{n_r} x_j^{m_l}(1 - x_j)^{m_r}}{n_l! n_r! m_l! m_r!}, \end{aligned} \tag{G1}$$

where $n_{l,r}$ and $m_{l,r}$ are the number of particles to the left/right of the two tagged particles $i$ and $j$. Here we want to focus on the ensemble-average reduced pair correlation function $P^{ij}_{\rm eq}(x_i, x_j)/(P_{\rm eq}(x_i)P_{\rm eq}(x_j))$ depicted in figure G1 and corresponding table G1. The latter is in general different from 0, while the former goes to 0 in the limit $t \to \infty$. $P^{c,c+1}_{\rm eq}(x, y)$ depends on $N$ and for large $N$ changes monotonically from positive to negative correlations as a function of particle separation. At small $N$ the correlations becomes weaker with increasing separation, but remains positive. Intuitively, as one particle lies in-between, the dependence of $P^{c,c+2}_{\rm eq}$ on the interparticle separation is for large $N$ non-monotonic, going from perfectly anticorrelated to correlated and back to anti-

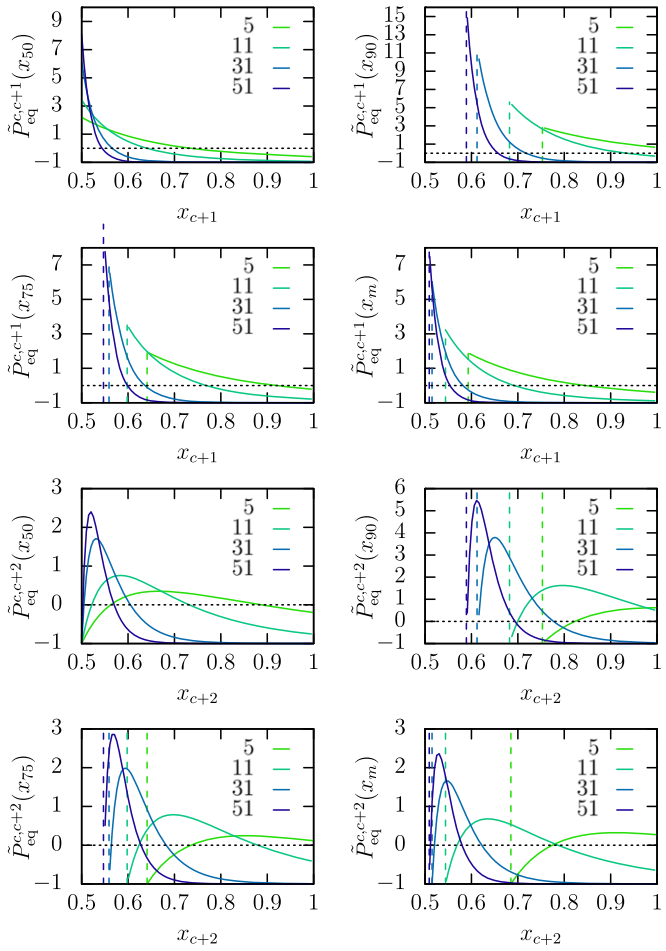


**Figure G1.** $P^{ij}_{\rm eq}(x_i,\, x_j)$ between the central particle $c$ and the right nearest and next-nearest neighbor, $c+1$ and $c+2$ respectively, when the central particle is tagged at $x_c = x_{50}, x_{75}, x_{90}$ and when $x_c = x_m$ (see table G1 for the exact positions). The vertical dashed lines are drawn at the position of the central particle (see table G1) to denote the non-crossing boundary condition.

**Table G1.** Reference points for the results of figure G1.

| $N$ | $x_{50}$ | $x_{75}$ | $x_{90}$ | $x_m$ |
|---|---|---|---|---|
| 5 | 0.500 | 0.651 | 0.753 | 0.593 |
| 11 | 0.500 | 0.598 | 0.682 | 0.544 |
| 31 | 0.500 | 0.559 | 0.612 | 0.515 |
| 51 | 0.500 | 0.547 | 0.589 | 0.509 |

correlation. At low $N$ $P^{c,c+2}_{\rm eq}$ depends non-trivially on the interparticle separation, such that the aforementioned terminal anticorrelation disappears for small enough $N$. Notably, for $x_c = x_{90}$ the correlations are much stronger, which suggest that more extensive excursions are entropically penalized as they demand collective fluctuations.

## Appendix H. Two-tag correlation function of local times

In the main text (in particular in figure 3) we analyzed one-point two-particle histories $\tilde{C}^{c,c+1,2}_{x_m x_m}(t)$ at the respective mid-point positions $x_m$ listed in table H1.

To gain further insight we also compute the first and central-particle two-point reduced correlation functions of local times $\tilde{C}^{1,1}_{xy}(t)$ and $\tilde{C}^{c,c}_{xy}(t)$ with $x$ and $y$ given in table H2. Figure H1. In the left plot we show the self-reduced reveals weak anti-correlations at short times $t$ turning to weak correlations at longer $t$, before reaching the LD limit of uncorrelated histories. As already mentioned in the main text, the correlations for the outer particles are weak and become weaker with increasing number of particles $N$, since the outer particles are constrained between the reflecting

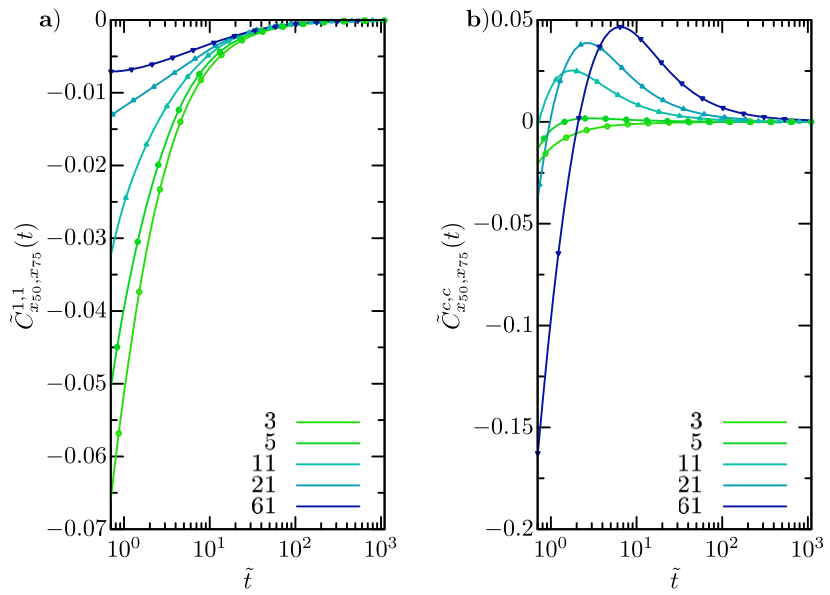


**Figure H1.** (a) $\tilde{C}^{1,1}_{x_{50}y_{75}}(t)$ of the first particle and (b) $\tilde{C}^{c,c}_{x_{50}y_{75}}(t)$ of the central particle.

**Table H1.** The location of the midpoint between the central particle and the right nearest and second nearest neighbors used in figure 3 in the main text.

| $N$ | $x_m$ | $y_m$ |
|---|---|---|
| 5 | 0.593 | 0.685 |
| 7 | 0.567 | 0.635 |
| 9 | 0.553 | 0.606 |
| 11 | 0.544 | 0.588 |
| 21 | 0.523 | 0.546 |
| 31 | 0.515 | 0.531 |
| 51 | 0.509 | 0.519 |
| 61 | 0.508 | 0.516 |
| 71 | 0.507 | 0.514 |
| 101 | 0.505 | 0.510 |

**Table H2.** Reference points for the results of figure H1.

| | First | | Central | |
|---|---|---|---|---|
| $N$ | $x_{50}$ | $x_{75}$ | $x_{50}$ | $x_{75}$ |
| 3 | 0.206 | 0.370 | 0.500 | 0.673 |
| 5 | 0.129 | 0.242 | 0.500 | 0.641 |
| 11 | 0.061 | 0.118 | 0.500 | 0.598 |
| 21 | 0.032 | 0.064 | 0.500 | 0.572 |
| 61 | 0.011 | 0.022 | 0.500 | 0.544 |

wall and the right nearest neighbor. In the case of the central particle we observe further evidence of the emergence of persistent collective fluctuations at higher densities, observed and described in the main text. Notably here even near-equilibrium fluctuations reveal signatures of collective behavior in the form of persistent histories (note that we are tagging at $x_{50}$ and $x_{75}$), i.e. $\tilde{C}^{c,c}_{x_{50},x_{75}}(t)$ turns from purely negative to weakly positive correlations.

## References

[1] Hodgkin A L and Keynes R D 1955 *J. Physiol.* **128** 61
Hummer G, Rasaiah J C and Noworyta J P 2001 *Nature* **414** 188
Beckstein O and Sansom M S P 2003 *Proc. Natl Acad. Sci. USA* **100** 7063

[2] Lomholt M A, Ambjörnsson T and Metzler R 2005 *Phys. Rev. Lett.* **95** 260603
Li G-W, Berg O G and Elf J 2009 *Nat. Phys.* **5** 294
Mahmutovic A, Berg O G and Elf J 2015 *Nucl. Acids Res.* **43** 3454
Shvets A A and Kolomeisky A B 2016 *J. Phys. Chem. Lett.* **7** 2502
[3] Kärger J and Ruthven D 1992 *Diffusion in Zeolites and Other Microporous Solids* (New York: Wiley)
Chou T and Lohse D 1999 *Phys. Rev. Lett.* **82** 3552
[4] Richards P M 1977 *Phys. Rev.* B **16** 1393
[5] Lutz C, Kollmann M and Bechinger C 2004 *Phys. Rev. Lett.* **93** 026001
Chou C-Y and Eng B C 2006 *J. Chem. Phys.* **124** 044902
Lin B *et al* 2005 *Phys. Rev. Lett.* **94** 216001
[6] Locatelli E *et al* 2016 *Phys. Rev. Lett.* **117** 038001
Taloni A *et al* 2017 *Soft Matter* **13** 1096
[7] Harris T E 1965 *J. Appl. Probab.* **2** 323
[8] Lizana L and Ambjörnsson T 2008 *Phys. Rev. Lett.* **100** 100601
Lizana L and Ambjörnsson T 2009 *Phys. Rev.* E **80** 051103
[9] Percus J K 1974 *Phys. Rev.* A **9** 557
[10] Aslangul C 1998 *Europhys. Lett.* **44** 284
Flomenbom O and Taloni A 2008 *Europhys. Lett.* **83** 20004
van Beijeren H 1991 *J. Stat. Phys.* **63** 47
Leibovich N and Barkai E 2013 *Phys. Rev.* E **88** 032107
[11] Jepsen D W 1965 *J. Math. Phys.* **6** 405
Lebowitz J L and Percus J K 1967 *Phys. Rev.* **155** 122
Lebowitz J L and Sykes J 1972 *J. Stat. Phys.* **6** 157
van Beijeren H, Kehr K W and Kutner R 1983 *Phys. Rev.* B **28** 5711
Majumdar S N and Barma M 1991 *Phys. Rev.* B **44** 5306
Kollmann M 2003 *Phys. Rev. Lett.* **90** 180602
Taloni A and Marchesoni F 2006 *Phys. Rev. Lett.* **96** 020601
Gupta S, Majumdar S N, Godréche C and Barma M 2007 *Phys. Rev.* E **76** 021112
Illien P *et al* 2013 *Phys. Rev. Lett.* **111** 038102
Bénichou O *et al* 2013 *Phys. Rev. Lett.* **111** 260601
Sanders L P *et al* 2014 *New J. Phys.* **16** 11305
[12] Rödenbeck C, Kärger J and Hahn K 1998 *Phys. Rev.* E **57** 4382
[13] Barkai E and Silbey R 2009 *Phys. Rev. Lett.* **102** 050602
Barkai E and Silbey R 2010 *Phys. Rev.* E **81** 041129
[14] Lizana L *et al* 2010 *Phys. Rev.* E **81** 051118
[15] Krapivsky P L, Mallick K and Sadhu T 2014 *Phys. Rev. Lett.* **113** 078101
Krapivsky P L, Mallick K and Sadhu T 2015 *J. Stat. Phys.* **160** 885
[16] Hegde C, Sabhapandit S and Dhar A 2014 *Phys. Rev. Lett.* **113** 120601
Sadhu T and Derrida B 2015 *J. Stat. Mech.* **2015** P09008
[17] Bénichou O and Desbois J 2015 *J. Stat. Mech.* **2015** P03001
[18] Stroock D W and Varadhan S R S 2006 *Multidimensional Diffusion Processes* (Berlin: Springer)
[19] Kac M 1949 *Trans. Am. Math. Soc.* **65** 1
[20] Lamperti J 1958 *Trans. Am. Math. Soc.* **88** 380
Godréche C and Luck J M 2001 *J. Stat. Phys.* **104** 489
Ehrhardt G C M A, Majumdar S N and Bray A J 2004 *Phys. Rev.* E **69** 016106
Comtet A, Desbois J and Texier C 2005 *J. Phys.* A **38** R341
Majumdar S N 2005 *Curr. Sci.* **89** 2076
Margolin G and Barkai E 2005 *Phys. Rev. Lett.* **94** 080601
Bel G and Barkai E 2005 *Phys. Rev. Lett.* **94** 240602
Barkai E 2006 *J. Stat. Phys.* **123** 883
Bénichou O *et al* 2005 *J. Phys.* A **38** 7205
Zatloukal V 2017 *Phys. Rev.* E **95** 052136
[21] Majumdar S N and Comtet A 2005 *J. Stat. Phys.* **119** 777
Schehr G, Majumdar S N, Comtet A and Randon-Furling J 2008 *Phys. Rev. Lett.* **101** 150601
Schehr G 2012 *J. Stat. Phys.* **149** 385
Kundu A, Majumdar S N and Schehr G 2013 *Phys. Rev. Lett.* **110** 220602
[22] Majumdar S N and Comtet A 2002 *Phys. Rev. Lett.* **89** 060601
Sabhapandit S, Majumdar S N and Comtet A 2006 *Phys. Rev.* E **73** 051102
[23] Chetrite R and Gawędzki K 2008 *Commun. Math. Phys.* **282** 469
[24] Dyson F J 1949 *Phys. Rev.* **75** 486
[25] Gardiner C W 1985 *Handbook of Stochastic Methods for Physics, Chemistry and the Natural Sciences* (Berlin: Springer)
[26] Majumdar S N and Bray A J 2002 *Phys. Rev.* E **65** 51112
Hartich D and Seifert U 2016 *Phys. Rev.* E **94** 042416
[27] Korepin V E, Bogoliubov N M and Izergin A G 1993 *Quantum Inverse Scattering Method and Correlation Functions* (Cambridge: Cambridge University Press)
[28] Ritort F and Sollich P 2003 *Adv. Phys.* **52** 219
[29] Hartich D and Godec A 2018 arXiv:1802.10046; arXiv:1802.10049
[30] Kleinert H 2009 *Path Integrals In Quantum Mechanics, Statistics, Polymer Physics, And Financial Markets* 5th edn (Singapore: World Scientific)
[31] Weber M F and Frey E 2017 *Rep. Prog. Phys.* **80** 046601
[32] Majumdar S N and Dean D S 2002 *Phys. Rev.* E **66** 041102